Taco complex-templated highly regio- and stereo-selective photodimerization of a coumarin-containing crown ether

Peifa Wei, Haoze Wang, Kecheng Jie and Feihe Huang*

State Key Laboratory of Chemical Engineering, Center for Chemistry of High-Performance & Novel Materials, Department of Chemistry, Zhejiang University, Hangzhou 310027, P. R. China

Electronic Supplementary Information

1. Materials and methods

Compounds **S1**,[S1] **3**,[S2] and **4**[S3] were synthesized according to literature procedures. All reagents were commercially available and used as supplied without further purification. Solvents were either employed as purchased or dried according to procedures described in the literature. NMR spectra were recorded with a Bruker Advance DMX 400 spectrophotometer with the deuterated solvent as the lock and the residual solvent or TMS as the internal reference. ^{1}H and ^{13}C NMR chemical shifts are reported relative to residual solvent signals. The two-dimensional diffusion-ordered (2D DOSY) NMR spectra and H-H correlation NMR spectra (2D COSY) were recorded on a Bruker DRX500 spectrometer. Mass spectra were recorded on a Micromass Quattro II triple-quadrupole mass spectrometer using electrospray ionization and analyzed with the MassLynx software suite or a Bruker Esquire 3000 plus mass spectrometer (Bruker-Franzen Analytik GmbH, Bremen, Germany) equipped with an ESI interface and an ion trap analyzer. High-resolution mass spectrometry experiments were performed with a Bruker 7-Tesla FT-ICR mass spectrometer equipped with an electrospray source (Billerica, MA, USA). UV-vis spectroscopy was performed on a Shimadzu UV-2550 instrument at room temperature. The melting points were collected on a SHPSIC WRS-2 automatic melting point apparatus. FT-IR spectra were taken with potassium bromide pellets on a TENSOR 27 spectrometer. The dimer was formed by UV irradiation with a CHF-XM-500W UV lamp with a 365 nm filter. The crystal data were collected on an Oxford Diffraction Xcalibur Atlas Gemini ultra instrument. The crystal structures were solved by SHELXS-97[S4] and refined by SHELXL-97.[S5]

2. *Synthetic procedures*

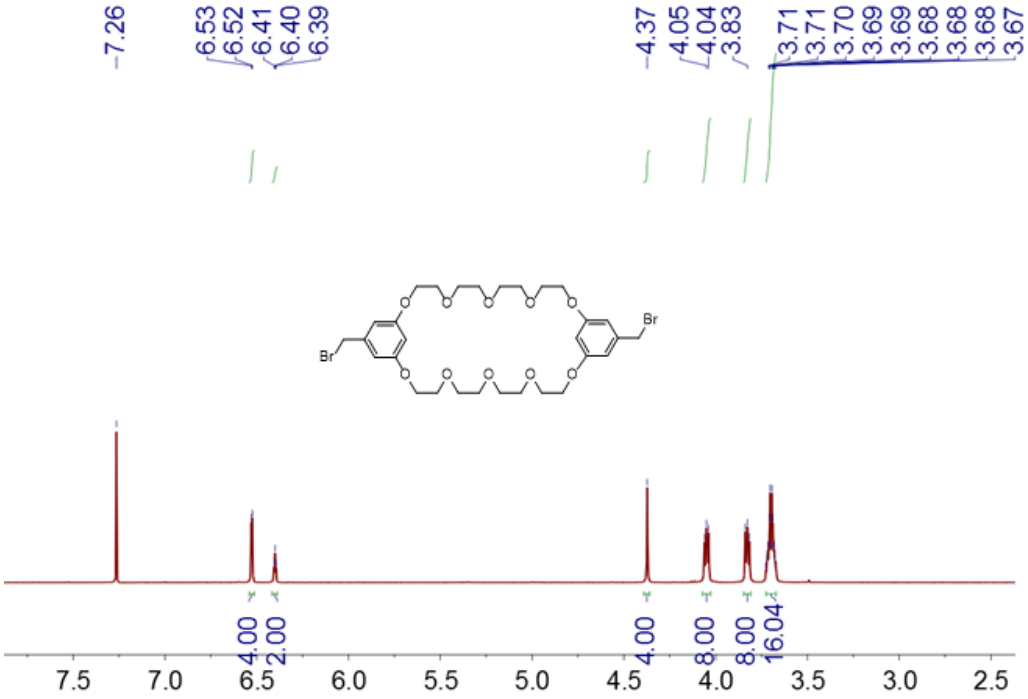

Fig. S1. ^{1}H NMR spectrum (400 MHz, $CDCl_3$, 293 K) of **S1**.

Scheme S1. Synthetic route to **1**

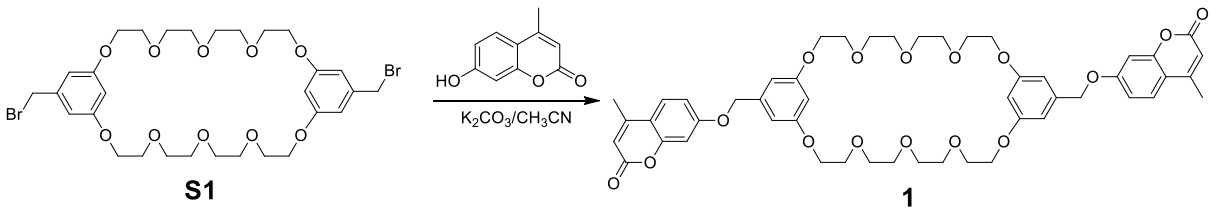

In a 200 mL round-bottomed flask were added **S1** (0.722 g, 1.00 mmol), 4-methylumbelliferone (0.704 g, 4.00 mmol), and K_2CO_3 (0.552 g, 4.00 mmol) in 100 mL of CH_3CN. After heating at reflux under N_2 for 12 h, the solvent was removed and CH_2Cl_2 was added. The mixture was washed with water and brine, and then purified by flash column chromatography (dichloromethane/methanol, 1:100 *v*/*v*) to afford **1** as a white solid (1.62 g, 36%), mp 111.2–112.1 °C. The ^{1}H NMR spectrum of **1** is shown in Fig. S2. ^{1}H NMR (400 MHz, $CDCl_3$, 293 K) δ (ppm): 7.45–7.47 (d, 2H, J = 8 Hz), 6.86–6.89 (m, 2H), 6.78–6.79 (d, 2H, J = 4 Hz), 6.53–6.54 (d, 4H, J = 4 Hz), 6.40–6.41 (t, 2H, J = 4 Hz), 6.10 (s, 2H), 4.97 (s, 4H), 4.03–4.05 (m, 8H), 3.81–3.84 (m, 8H), 3.67–3.71 (m, 16H), and 2.36 (s, 6H). The ^{13}C NMR spectrum of **1** is shown in Fig. S3. ^{13}C NMR (100 MHz, $CDCl_3$, 293 K) δ (ppm): 18.68, 67.61, 69.64, 70.24, 70.86, 70.87, 101.07, 101.95, 106.04, 72.18, 112.02, 112.79, 113.79, 125.59, 138.09, 152.57, 155.13, 160.22, 161.25, and 165.22. LRESIMS is shown in Fig. S4: *m*/*z* 935.6 for [**1** + Na]$^{+}$. HREIMS: *m*/*z* calcd for [**1** + Na]$^{+}$ $C_{50}H_{56}NaO_{16}$ 935.3466, found 935.3462, error –1 ppm.

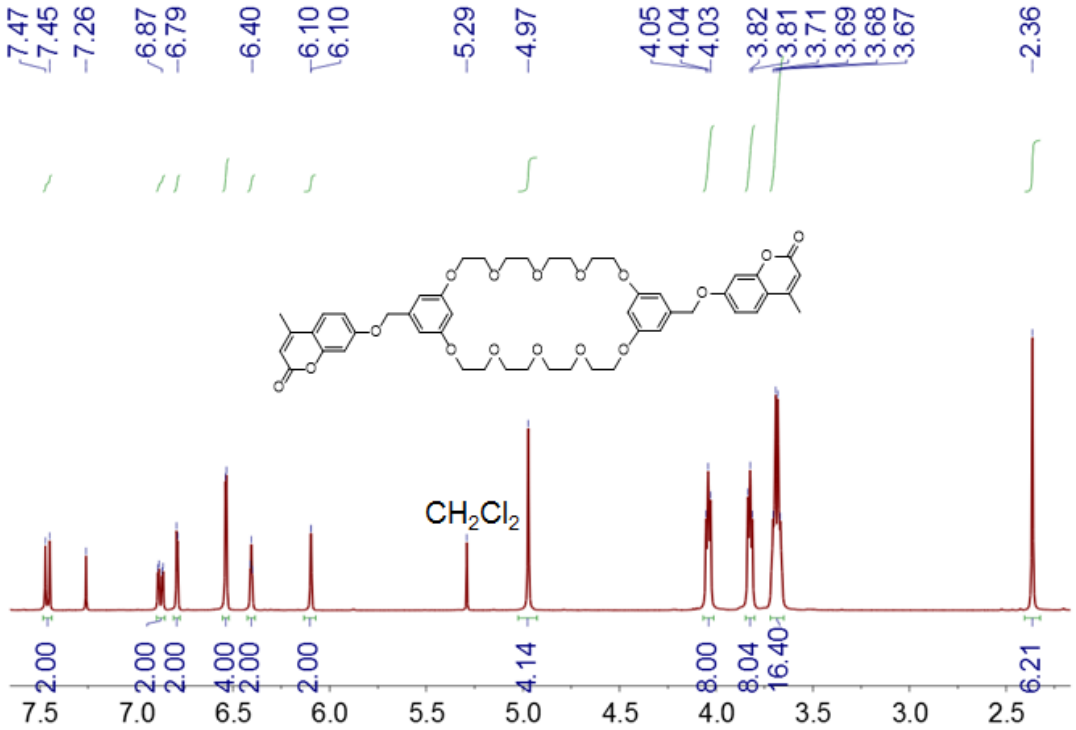

Fig. S2. ^{1}H NMR spectrum (400 MHz, $CDCl_3$, 293 K) of **1**.

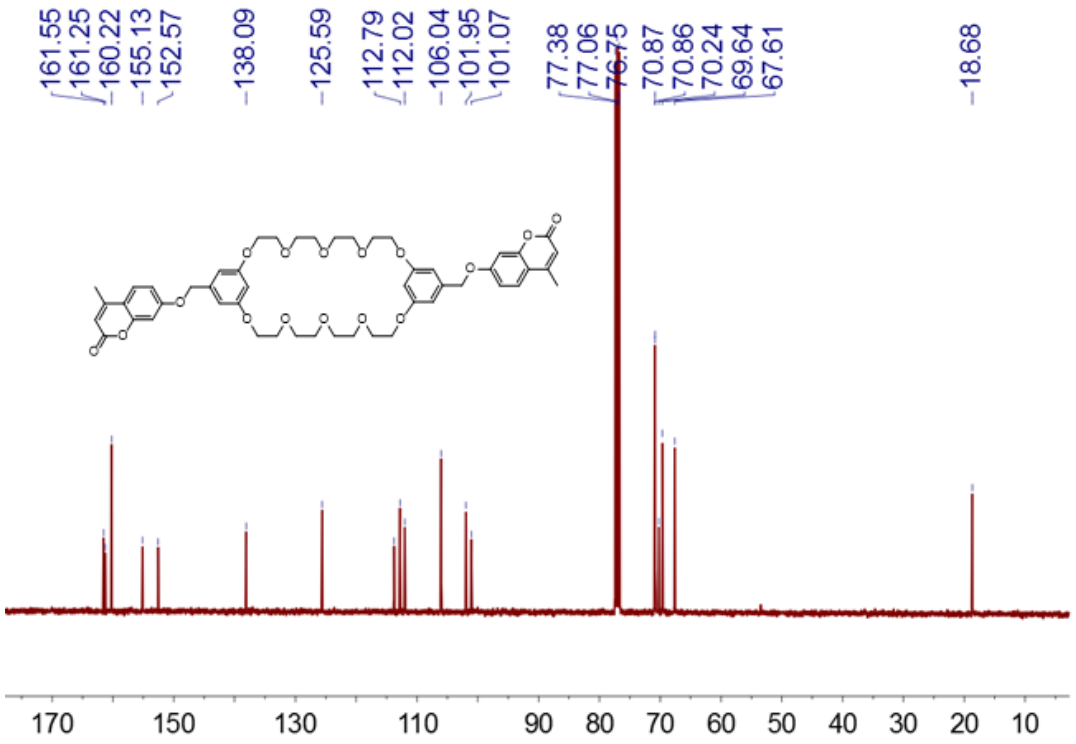

Fig. S3. ^{13}C NMR spectrum (100 MHz, $CDCl_3$, 293 K) of **1**.

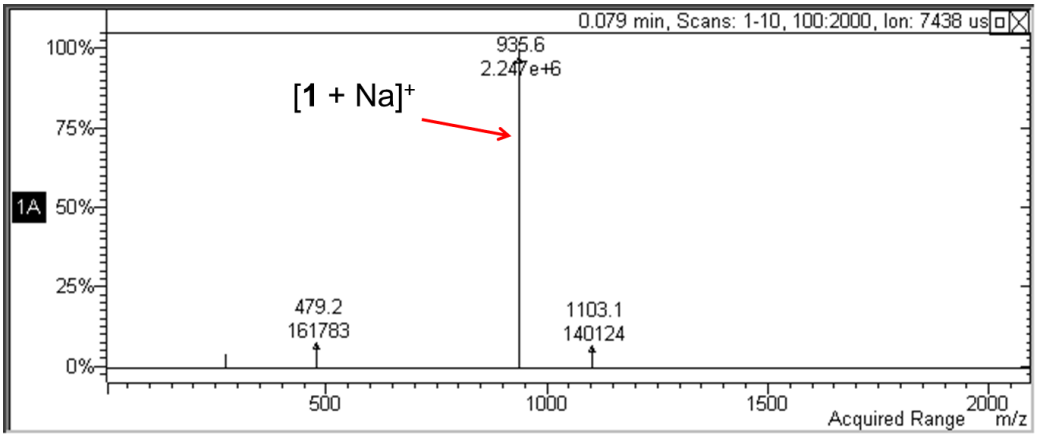

Fig. S4. Electrospray ionization mass spectrum of **1**.

3. *Host–guest complexation studies of **1**⊃**3** and **1**⊃**4***

3.1. *^{1}H NMR spectra of **1**⊃**3** and **1**⊃**4***

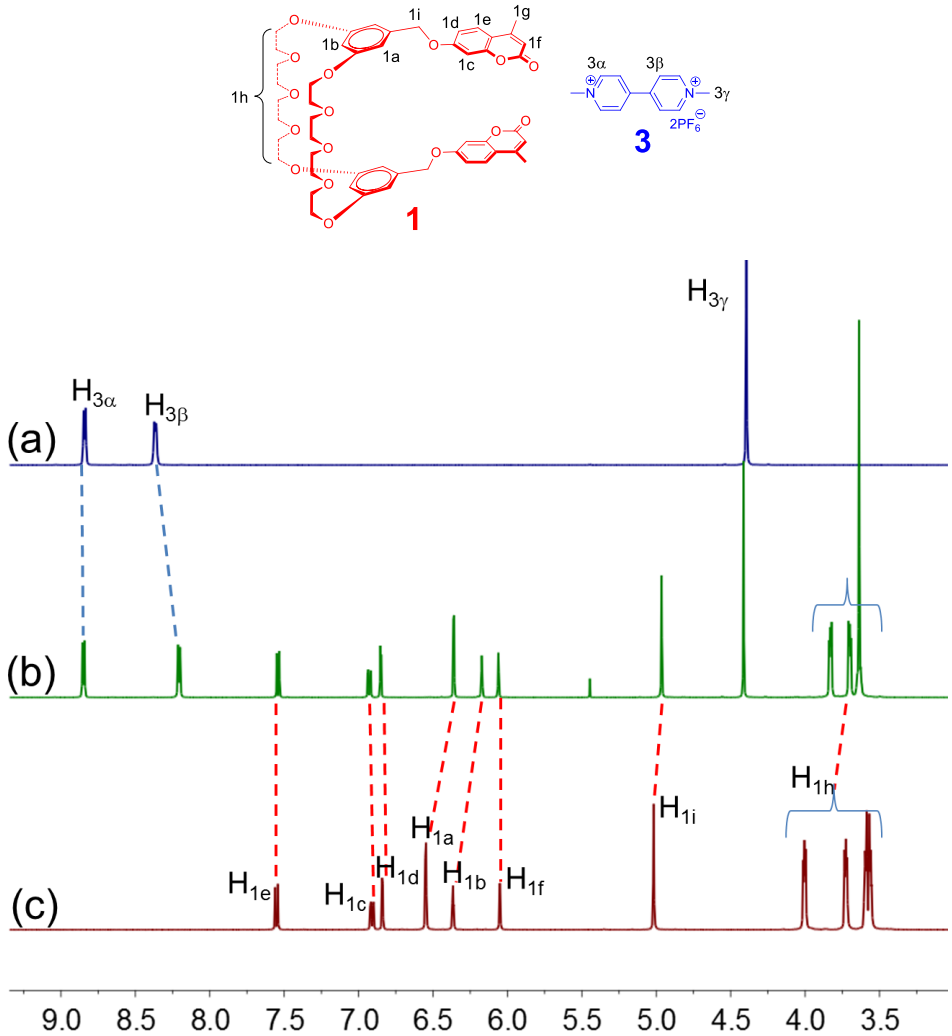

Fig. S5. Partial ^{1}H NMR spectra (400 MHz, $CDCl_3$, 293 K): (a) **3**; (b) **1**⊃**3**; (c) **1**. *c* = 10.0 mM.

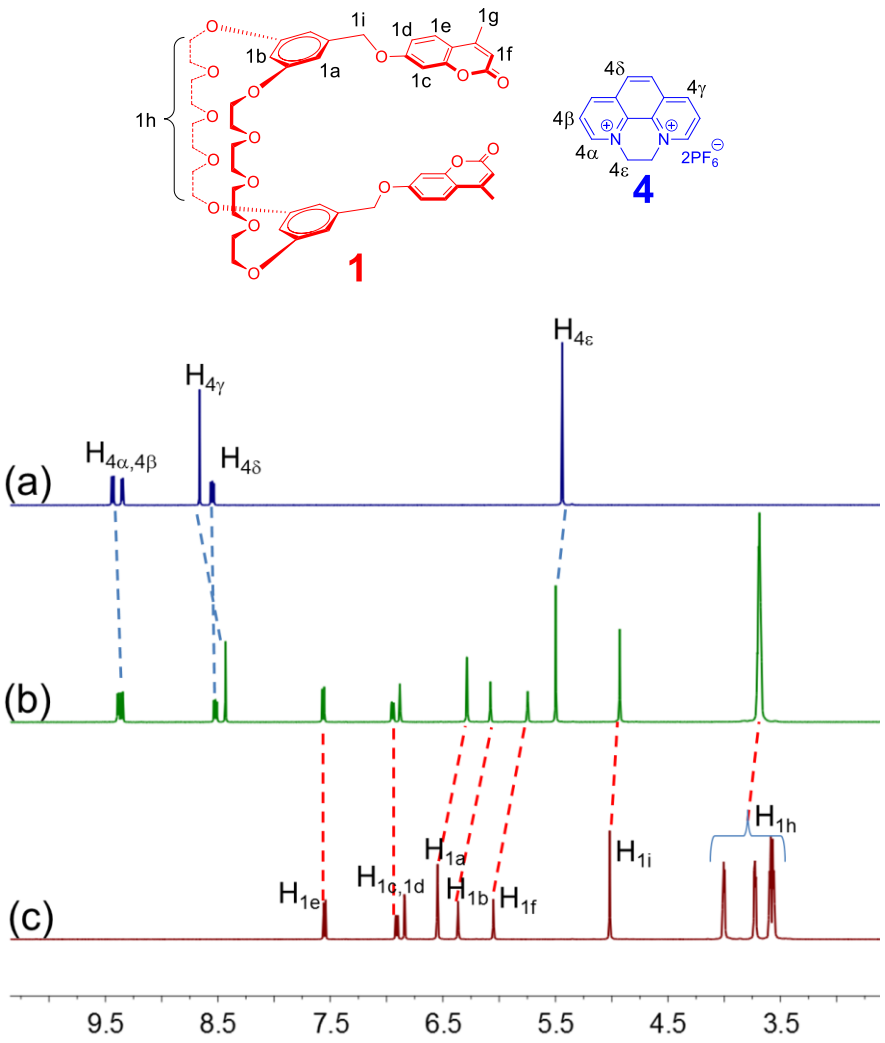

Fig. S6. Partial ^{1}H NMR spectra (400 MHz, $CDCl_3$, 293 K): (a) **4**; (b) **1**⊃**4**; (c) **1**. *c* = 10.0 mM.

*3.2. Job plots of **1**⊃**3** and **1**⊃**4** based on UV-vis spectroscopic data in acetone*

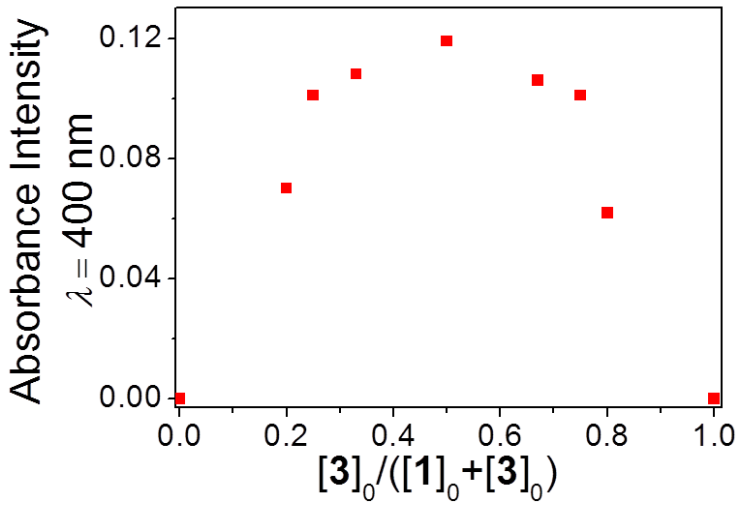

Fig. S7. Job plot showing the 1:1 stoichiometry of the complex between **1** and **3** in acetone. $[\mathbf{1}]_0 + [\mathbf{3}]_0$ = 2.00 mM. $[\mathbf{1}]_0$ and $[\mathbf{3}]_0$ are the initial concentrations of **1** and **3**.

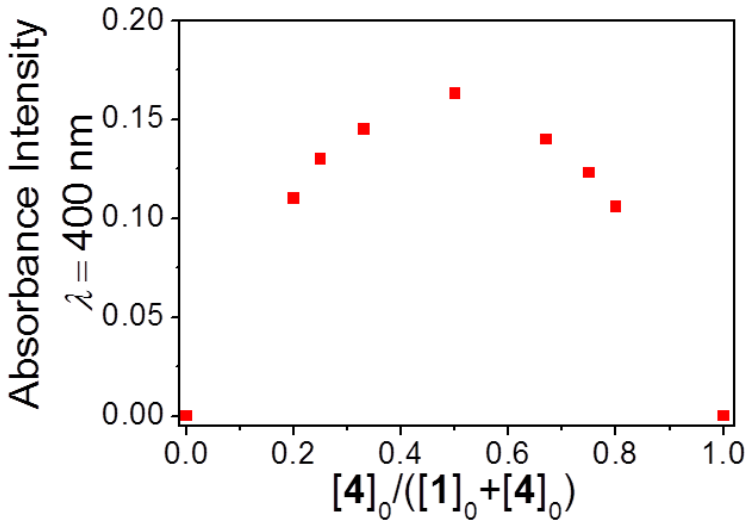

Fig. S8. Job plot showing the 1:1 stoichiometry of the complex between **1** and **4** in acetone. $[\mathbf{1}]_0 + [\mathbf{4}]_0 =$ 2.00 mM. $[\mathbf{1}]_0$ and $[\mathbf{4}]_0$ are the initial concentrations of **1** and **4**.

*3.3. Electrospray ionization mass spectra of host **1** with guest **3** or **4** in acetone*

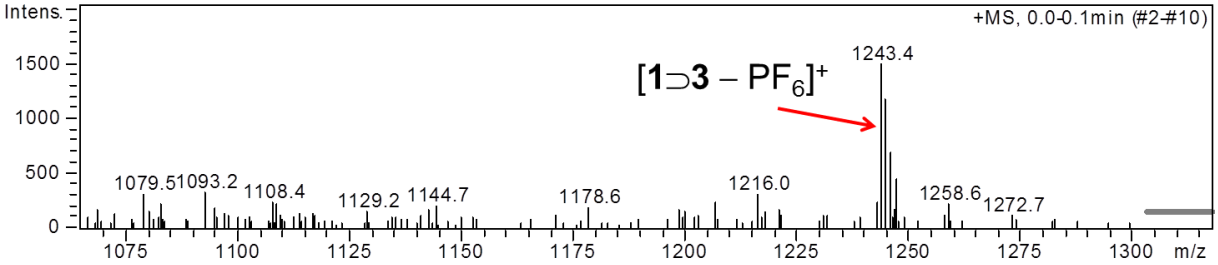

Fig. S9. The positive electrospray ionization mass spectrum of an equimolar mixture of **1** and **3** in acetone. Mass fragment at *m/z* 1243.4 for $[\mathbf{1}\supset\mathbf{3} - PF_6]^+$ confirmed the 1:1 complexation stoichiometry between **1** and **3**.

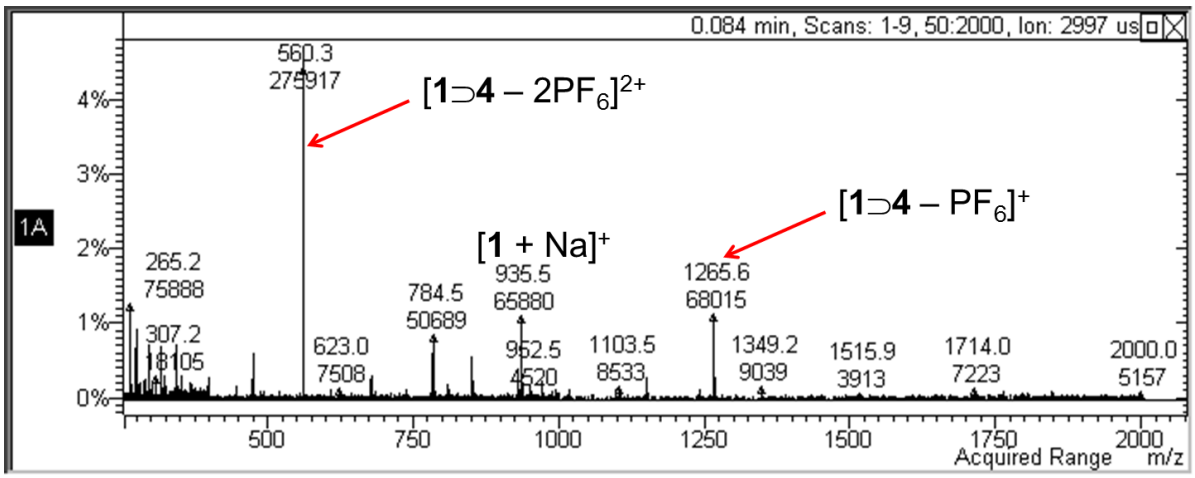

Fig. S10. The positive electrospray ionization mass spectrum of an equimolar mixture of **1** and **4** in acetone. Mass fragments at *m/z* 1265.6 for $[\mathbf{1}\supset\mathbf{4} - PF_6]^+$ and *m/z* 560.3 for $[\mathbf{1}\supset\mathbf{4} - 2PF_6]^{2+}$ confirmed the 1:1 complexation stoichiometry between **1** and **4**.

*3.4. Determination of association constants of complexes **1**⊃**3** and **1**⊃**4** in acetone*

The association constants (K_a) of complexes **1**⊃**3** and **1**⊃**4** were determined by probing the charge-transfer band of the complexes by UV-vis spectroscopy and employing a titration method. Progressive addition of an acetone solution with high guest concentration and low host concentration to an acetone solution with the same host concentration resulted in an increase of the intensity of the charge-transfer band of the complex. Treatment of the collected absorbance data with a non-linear curve-fitting program afforded the corresponding association constants (K_a): $(5.35 \pm 0.14) \times 10^2$ M^{-1} for **1**⊃**3** and $(3.21 \pm 0.25) \times 10^2$ M^{-1} for **1**⊃**4**.

The non-linear curve-fitting was based on the equation:

$$A = (A_\infty/[H]_0)\,(0.5[G]_0 + 0.5([H]_0+1/K_a)-(0.5\,([G]_0^2+(2[G]_0(1/K_a - [H]_0)) + (1/K_a + [H]_0)^2)^{0.5})) \quad \text{(Eq. S1)}$$

Wherein A is the absorption intensity of the charge-transfer band at $[G]_0$, A_∞ is the absorption intensity of the charge-transfer band when the host is completely complexed, $[H]_0$ is the fixed initial concentration of the host, and $[G]_0$ is the initial concentration of the guest.

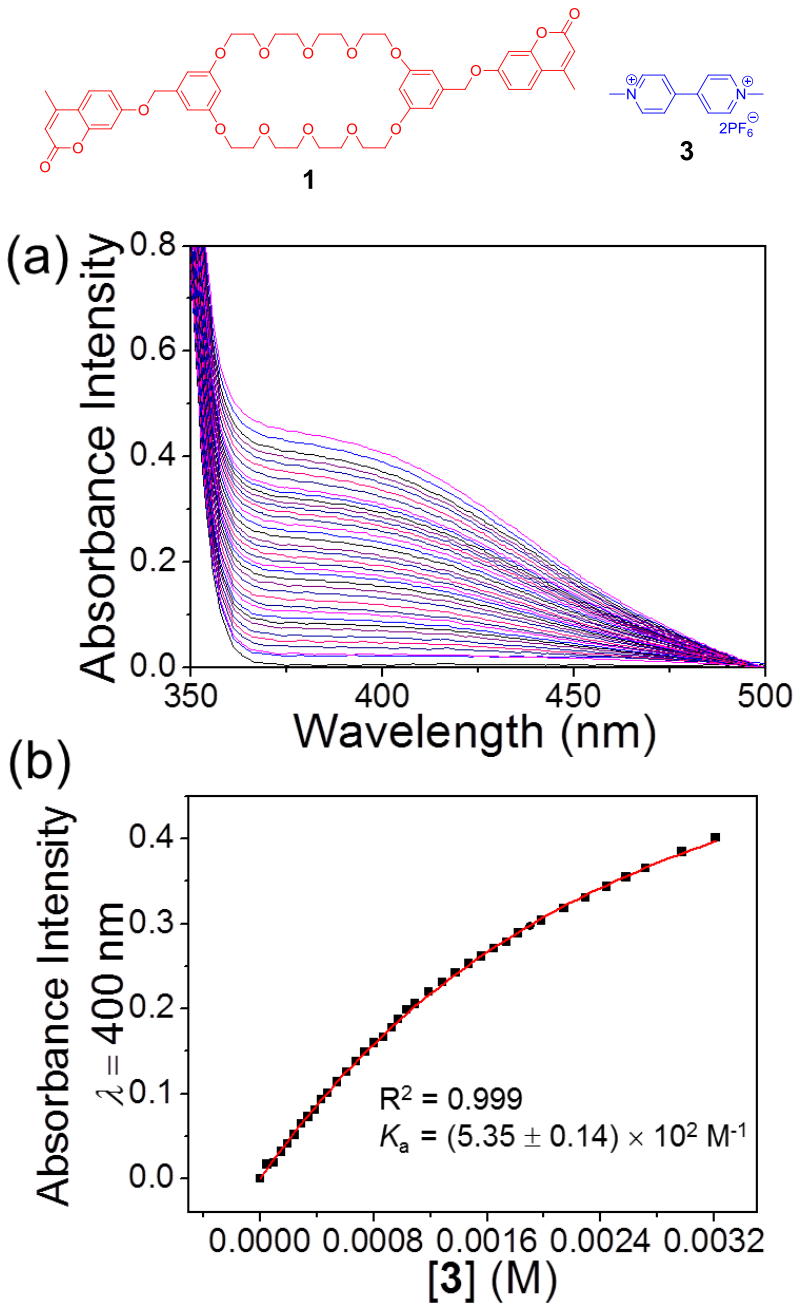

Fig. S11. (a) The absorption spectral changes of **1** (1.00 mM) upon addition of **3** and (b) the absorbance intensity changes at λ = 400 nm upon addition of **3** (from 0 to 3.20 mM). The red solid line was obtained from the non-linear curve-fitting using Eq. S1.

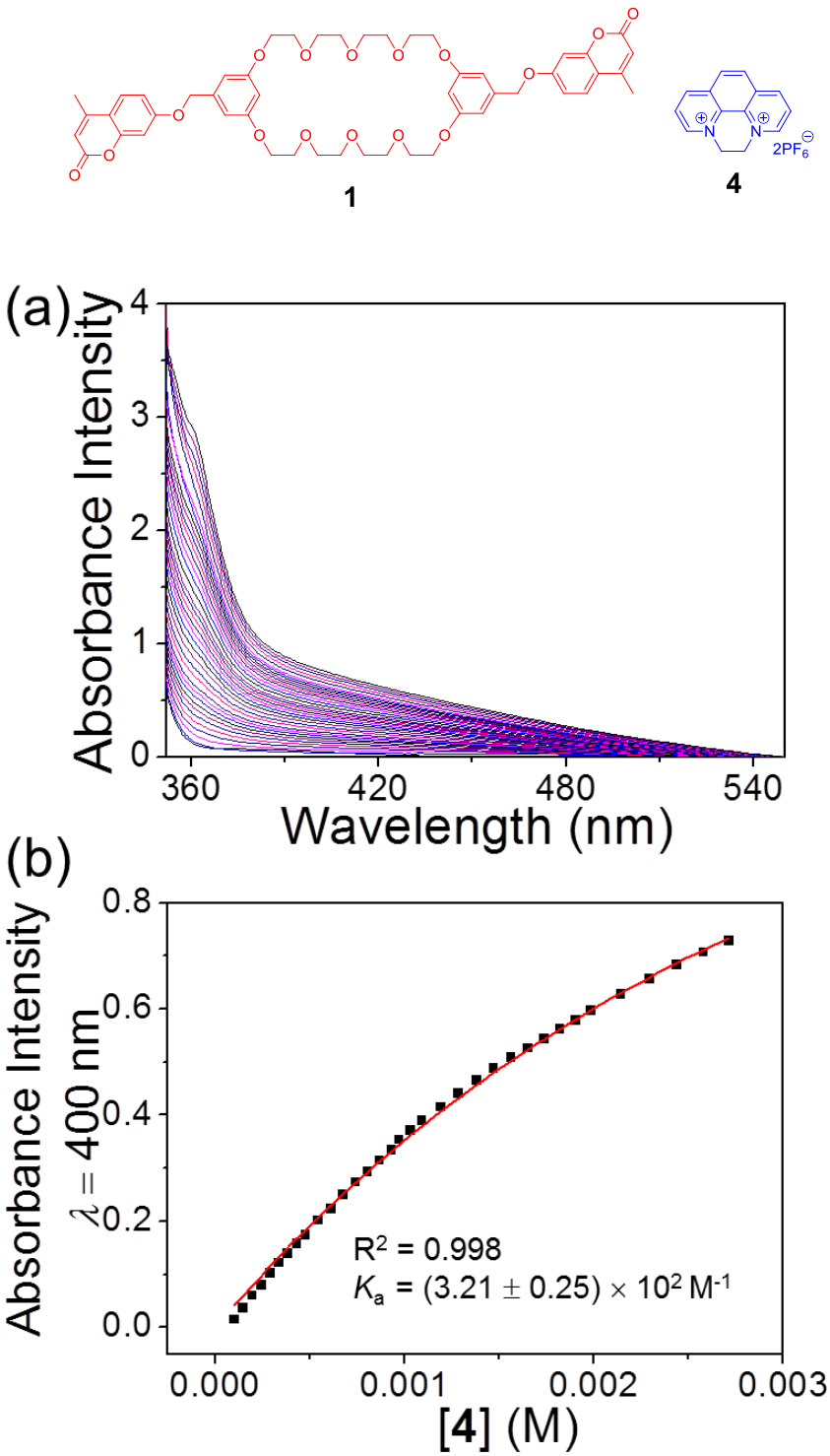

Fig. S12. (a) The absorption spectral changes of **1** (1.00 mM) upon addition of **4** and (b) the absorbance intensity changes at λ = 400 nm upon addition of **4** (from 0 to 2.80 mM). The red solid line was obtained from the non-linear curve-fitting using Eq. S1.

3.5. *X-ray crystal structure of* ***1⊃4*** *and energy optimized model of complex* ***1⊃3***

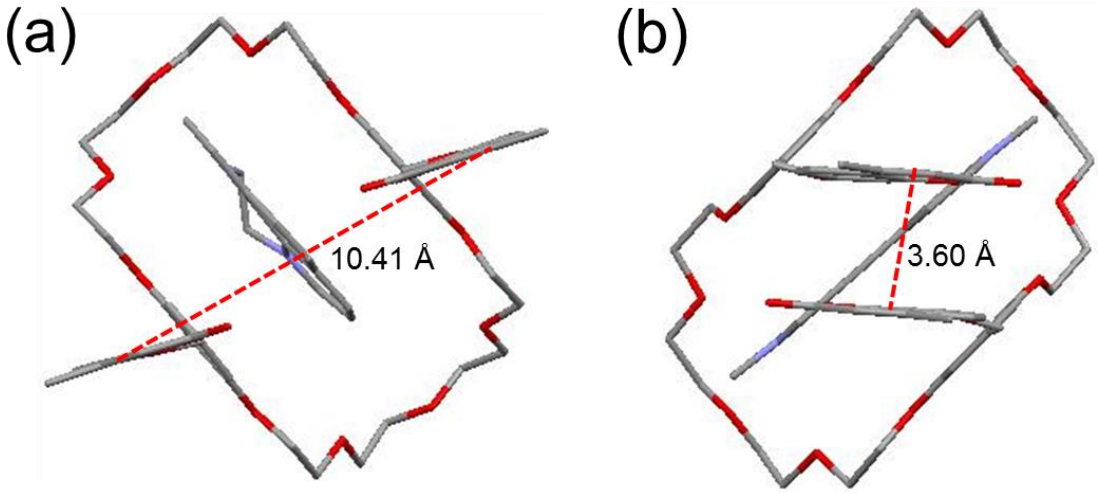

Fig. S13. (a) X-ray crystal structure of **1⊃4**; (b) the energy optimized (MM3) model of complex **1⊃3**. PF_6^- counterions and hydrogens were omitted for clarity.

3.6. *FT-IR spectra of complex* ***1⊃3*** *before and after photoirradiation*

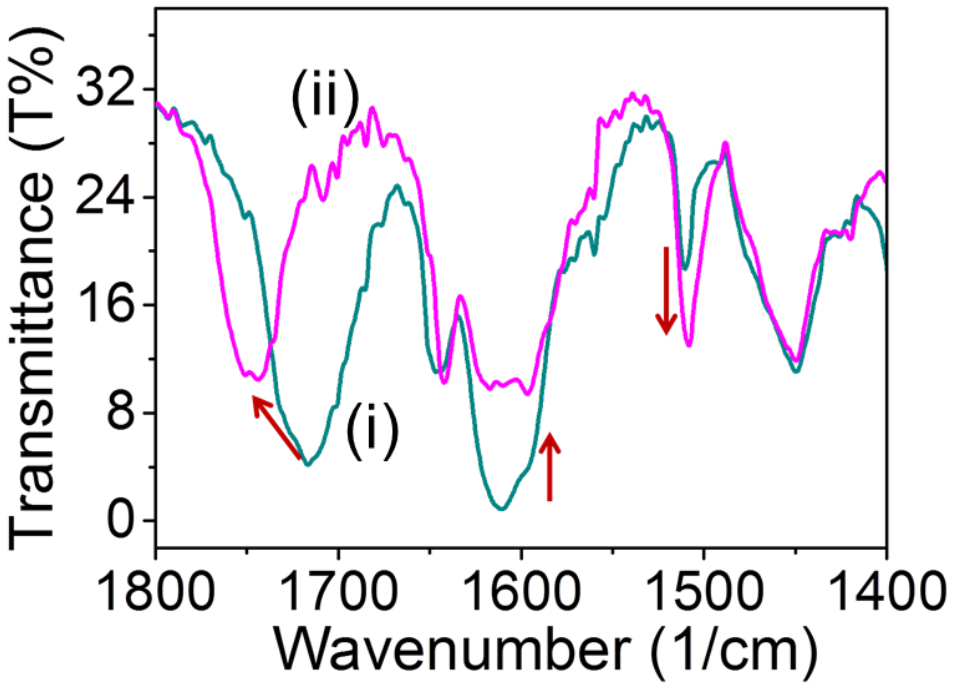

Fig. S14. FT-IR spectra: (i) complex **1⊃3**; (ii) after irradiation of (i) for 5 h. λ = 365 nm.

4. Taco complex template-induced selective photodimerization of coumarin groups

Scheme S2. Routes for the photodimerization

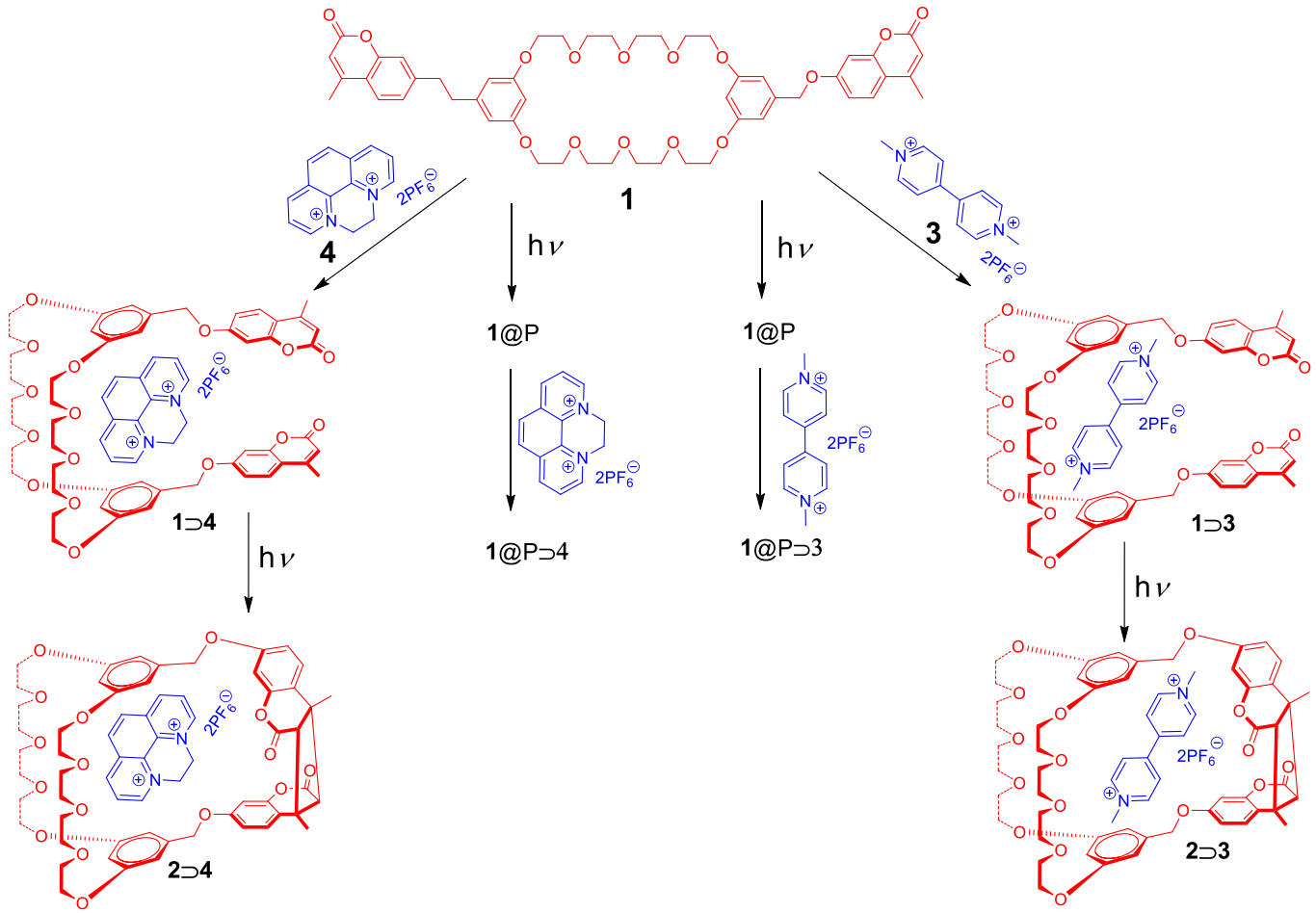

Two methods were used for the photodimerization process:

1) Host–guest complexes **1**⊃**3** and **1**⊃**4** were formed, so the coumarin groups in taco-type assemblies (Scheme S2) would be preoriented for the regio- and stereo-selective formation of the *syn head-to-tail* isomer in photochemically induced [2 + 2] cycloaddition reaction, thereby reducing the number of possible isomers from four to only one;
2) The solutions of host **1** without guests were irradiated for 6 hours, then guests **3** and **4** were added into the solutions; more than one [2 + 2] cycloaddition isomers were obtained.

*4.1. Photographs of solutions of **1**⊃**3**, (**1**⊃**3**)@P, **1**⊃**4**, and (**1**⊃**4**)@P*

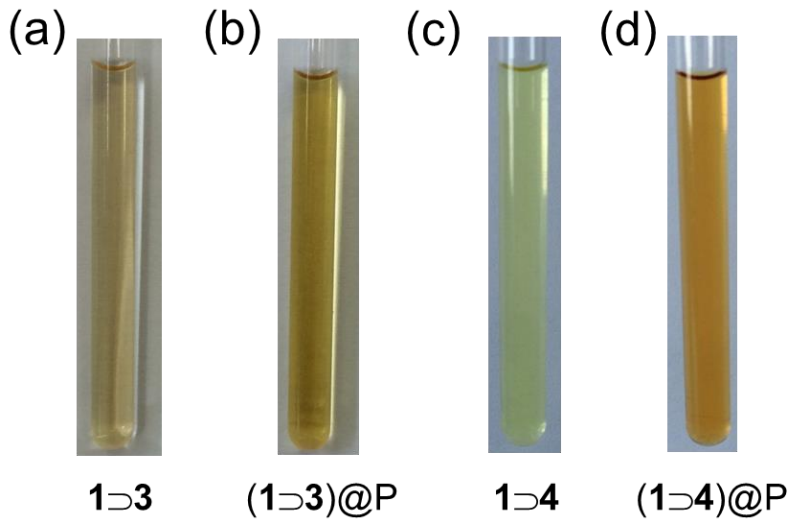

Fig. S15. Photographs of acetonitrile solutions: (a) **1**⊃**3**; (b) (**1**⊃**3**)@P; (c) **1**⊃**4**; (d) (**1**⊃**4**)@P.

.

*4.2. Electrospray ionization mass spectra of (**1**⊃**3**)@P and (**1**⊃**4**)@P in acetonitrile*

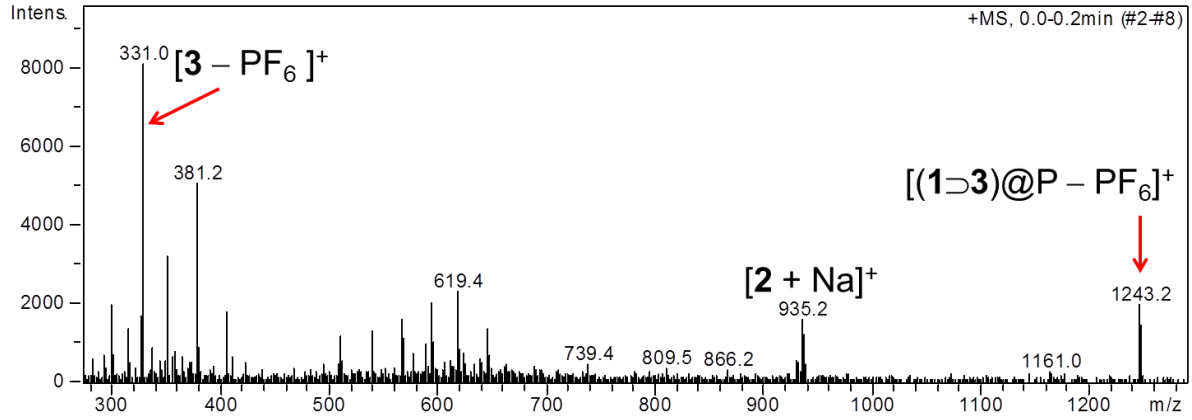

Fig. S16. The positive electrospray ionization mass spectrum of an equimolar mixture of **1** and **3** in acetonitrile after photoirradiation. Mass fragment at *m/z* 1243.2 for [(**1**⊃**3**)@P – PF_6]$^+$ confirmed the 1:1 complex between guest **3** and the photodimerization product of **1**. Here the photodimerization product of **1** is **2**; **1** and **2** have the same molecular weight.

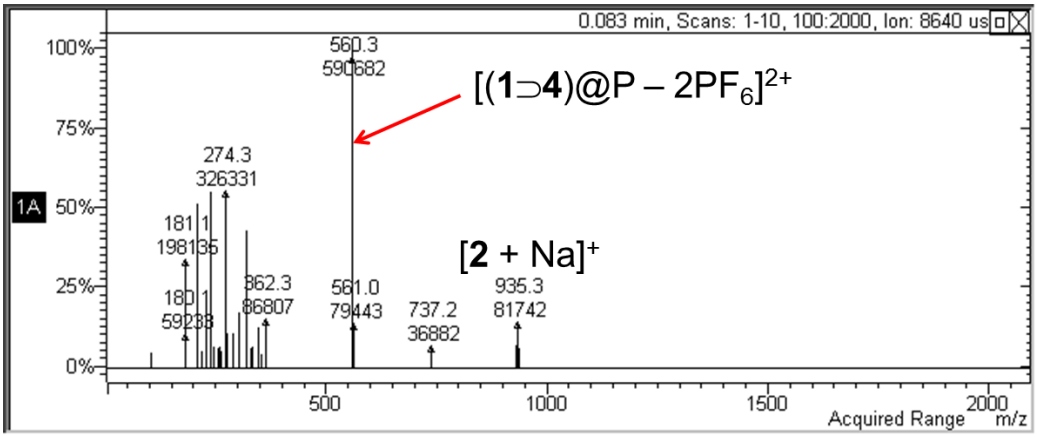

Fig. S17. The positive electrospray ionization mass spectrum of an equimolar mixture of **1** and **4** in acetonitrile after photo irradiation. The mass fragment at *m/z* 560.3 for $[(\mathbf{1}\supset\mathbf{4})@P - 2PF_6]^{2+}$ confirmed the 1:1 complex between guest **4** and the photodimerization product of **1**. Here the photodimerization product of **1** is **2**; **1** and **2** have the same molecular weight.

*4.3. COSY NMR spectra of **1**⊃**3** and (**1**⊃**3**)@P*

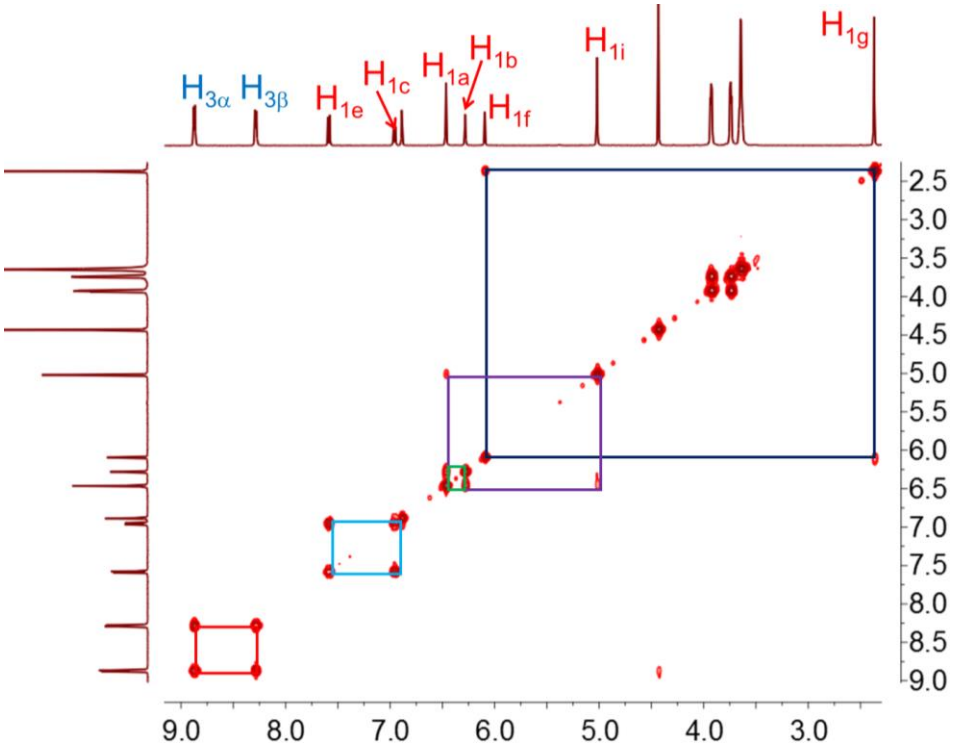

Fig.S18. Partial COSY NMR spectrum (500 MHz, $CDCl_3$, 293 K) of **1**⊃**3**. *c* = 10.0 mM.

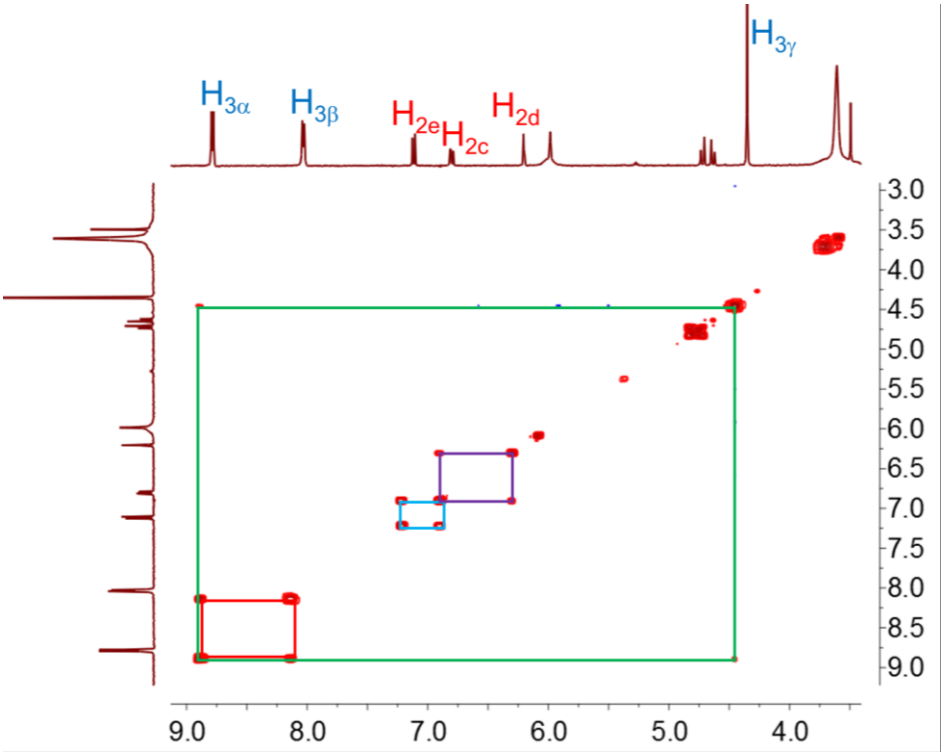

Fig. S19. Partial COSY NMR spectrum (500 MHz, $CDCl_3$, 293 K) of (**1**⊃**3**)@P. *c* = 10.0 mM.

*4.4. DOSY NMR spectra of **1**⊃**3** and (**1**@P)⊃**3***

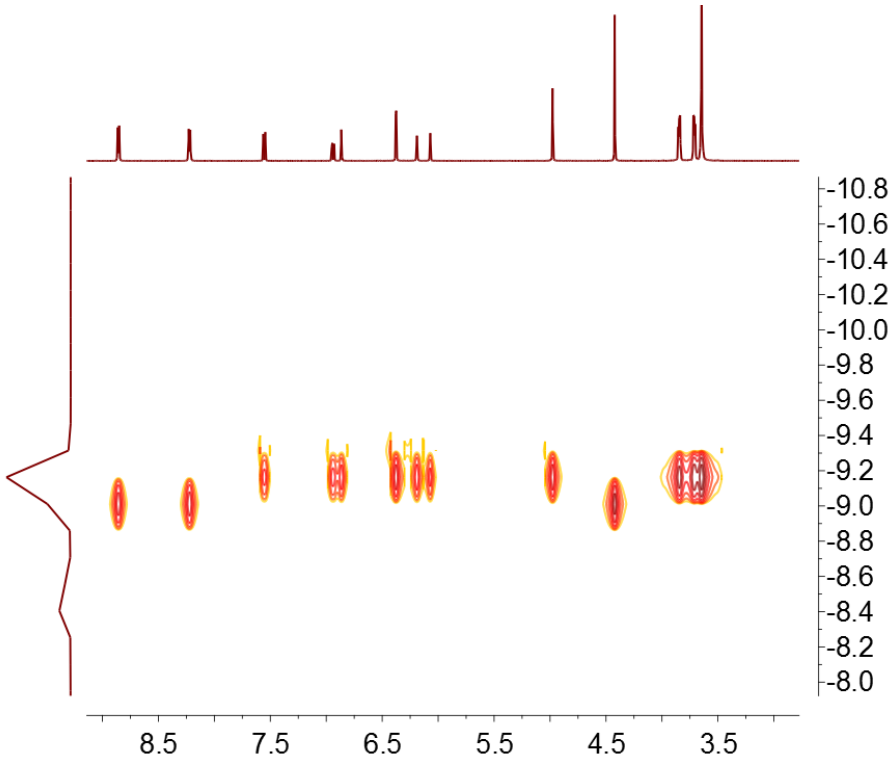

Fig. S20. Partial DOSY NMR spectrum (500 MHz, $CDCl_3$, 293 K) of **1**⊃**3**. *c* = 10.0 mM.

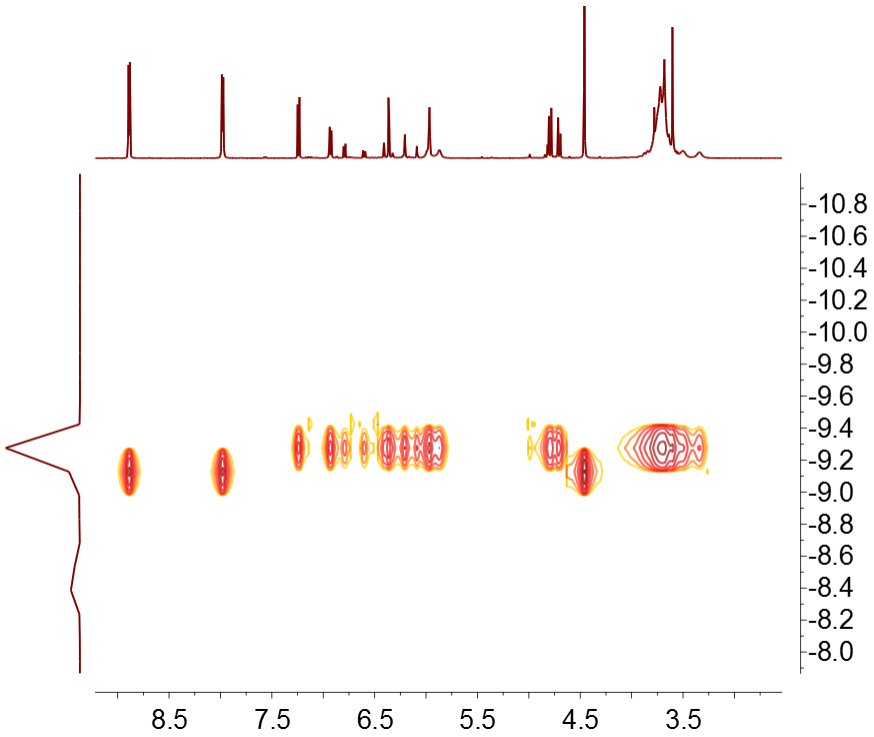

Fig. S21. Partial DOSY NMR spectrum (500 MHz, $CDCl_3$, 293 K) of (**1**@P)⊃**3**. *c* = 10.0 mM.

*4.5. Comparison of the ^{1}H NMR spectra of (**1**⊃**3**)@P and (**1**@P)⊃**3** at different concentrations*

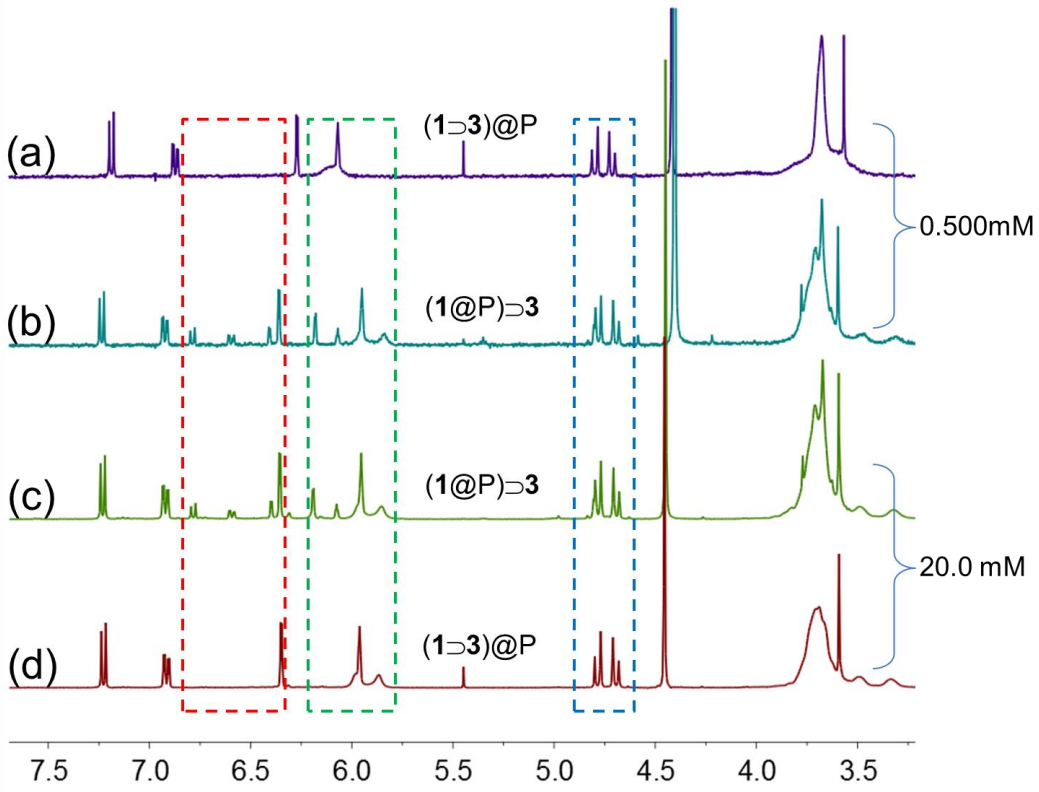

Fig. S22. Partial ^{1}H NMR spectra (500 MHz, $CDCl_3$, 293 K): (a) (**1**⊃**3**)@P, *c* = 0.500 mM; (b) (**1**@P)⊃**3**, *c* = 0.500 mM; (c) (**1**@P)⊃**3**, *c* = 20.0 mM; (d) (**1**⊃**3**)@P, *c* = 20.0 mM.

4.6. *Comparison of the ^{1}H NMR spectra of **1**, **1**⊃**3**, (**1**⊃**3**)@P, **2**⊃**3**, and (**1**@P)⊃**3***

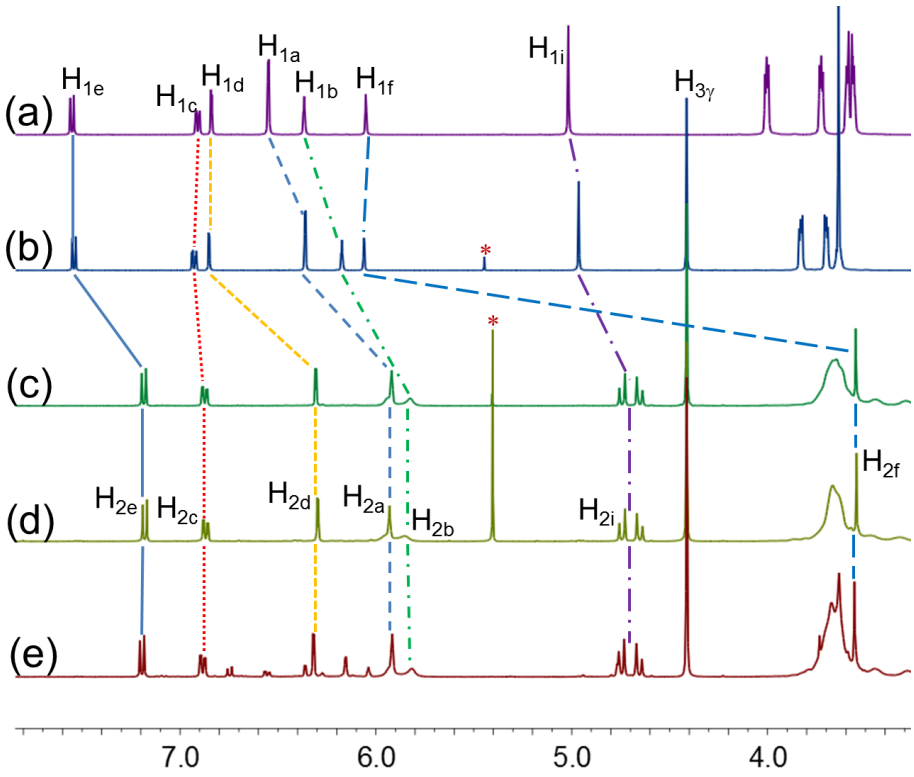

Fig. S23. Partial ^{1}H NMR spectra (500 MHz, $CDCl_3$, 293 K): (a) **1**; (b) **1**⊃**3**; (c) (**1**⊃**3**)@P; (d) **2**⊃**3**; (e) (**1**@P)⊃**3**. *c* = 10.0 mM. The prime ∗ in spectrum b and c denotes CH_2Cl_2.

5. *Host–guest complexation studies of **2**⊃**3** and **2**⊃**4***

5.1. *Synthesis and characterization of dimer **2***

Scheme S3. Synthetic route to **2**

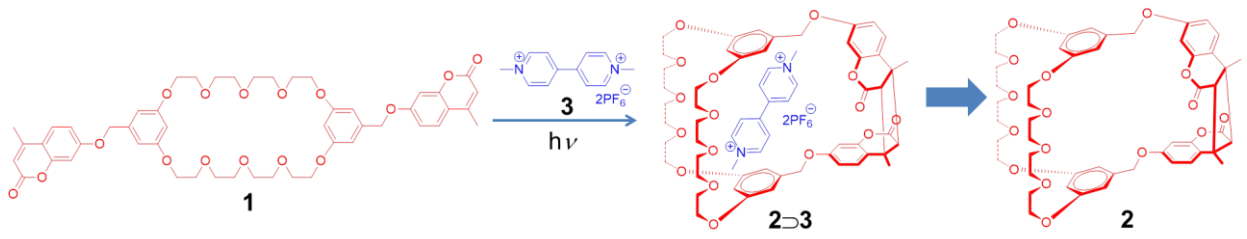

Equimolar **1** (36.4 mg, 40 mmol) and **3** (19.0, 40 mmol) in 2.00 mL acetonitrile were irradiated with a λ = 365 nm UV lamp for 6 hours. The solvent was evaporated by rotary evaporation and the resulting mixture was purified by flash column chromatography (dichloromethane/methanol, 1:50 *v*/*v*) to afford **2** as a white solid (35.6 g, 98.0%), mp 77.2–78.3 °C. The ^{1}H NMR spectrum of **2** is shown in Fig. S24. ^{1}H NMR (400

MHz, $CDCl_3$, 293 K) δ (ppm): 7.08–7.10 (d, 2H, J = 8 Hz), 6.72–6.74 (m, 2H), 6.39–6.40 (d, 4H, J = 4 Hz), 6.32–6.33 (t, 2H, J = 4 Hz), 6.06–6.07 (d, 2H, J = 4 Hz), 4.65–4.77 (m, 4H), 3.84–3.94 (m, 16H), 3.67–3.71 (m, 16H), 3.42 (s, 2H), and 1.68 (s, 6H). The ^{13}C NMR spectrum of **2** is shown in Fig. S25. ^{13}C NMR (100 MHz, $CDCl_3$, 293 K) δ (ppm): 31.19, 41.23, 55.40, 67.53, 69.75, 69.95, 70.66, 71.07, 101.06, 102.18, 105.67, 112.81, 114.12, 127.32, 138.11, 150.29, 159.43, 160.03, and 164.81. LRESIMS is shown in Fig. S26: m/z 935.5 for [**2** + Na]$^+$. HREIMS: m/z calcd for [**2** + Na]$^+$ $C_{50}H_{56}NaO_{16}$ 935.3466, found 935.3460, error –1 ppm.

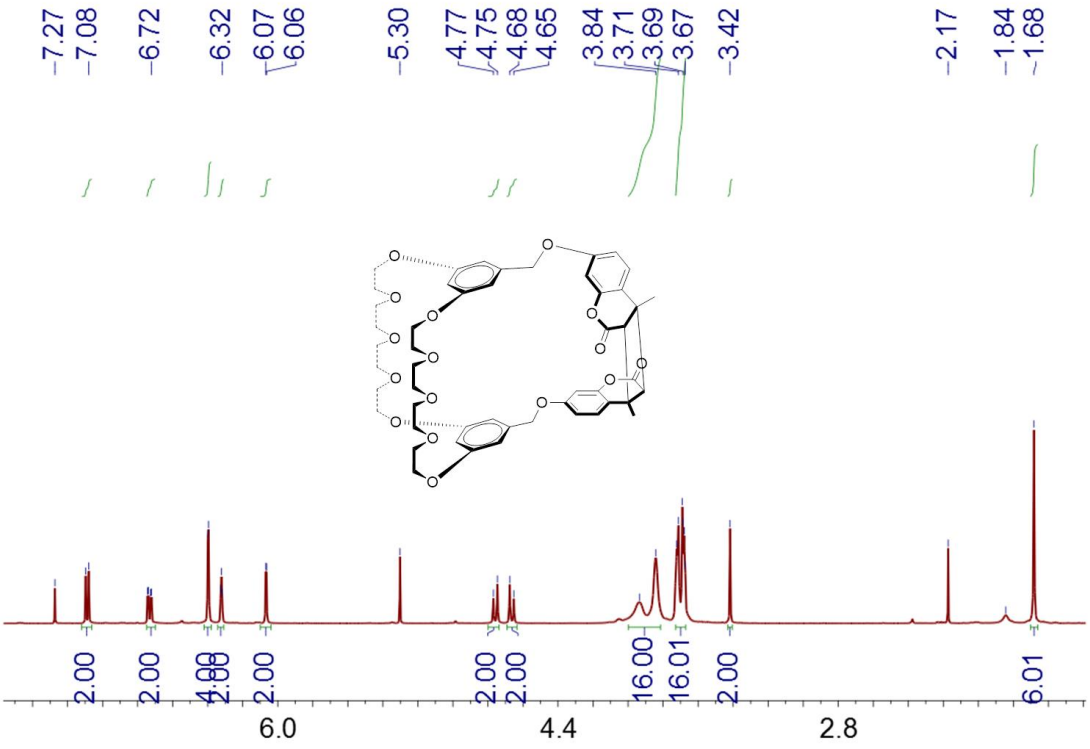

Fig. S24. ^{1}H NMR spectrum (400 MHz, $CDCl_3$, 293 K) of **2**.

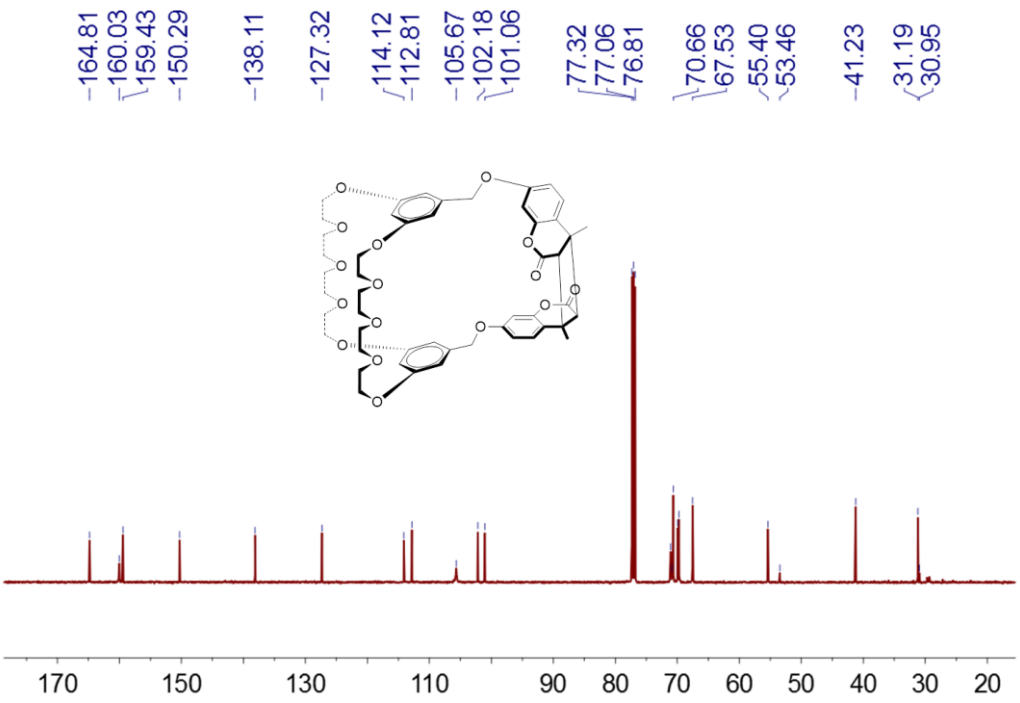

Fig. S25. ^{13}C NMR spectrum (100 MHz, $CDCl_3$, 293 K) of **2**.

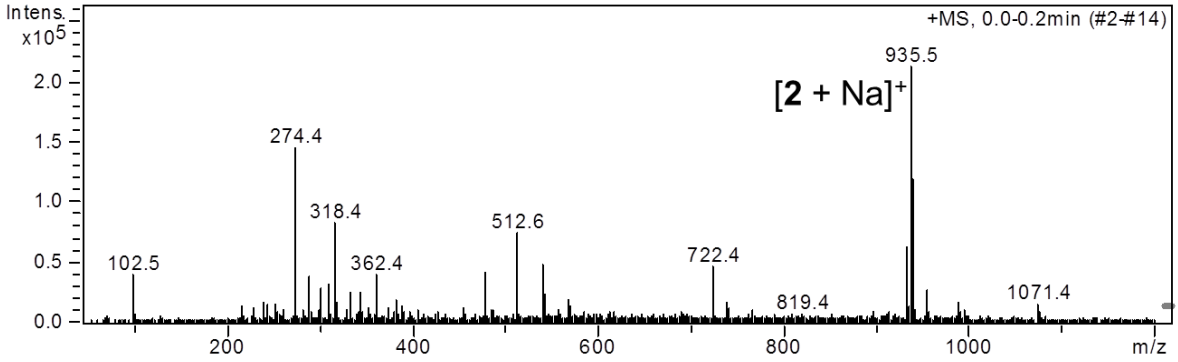

Fig.S26. Electrospray ionization mass spectrum of **2**.

*5.2. ^{1}H NMR spectra of **2**⊃**3** and **2**⊃**4***

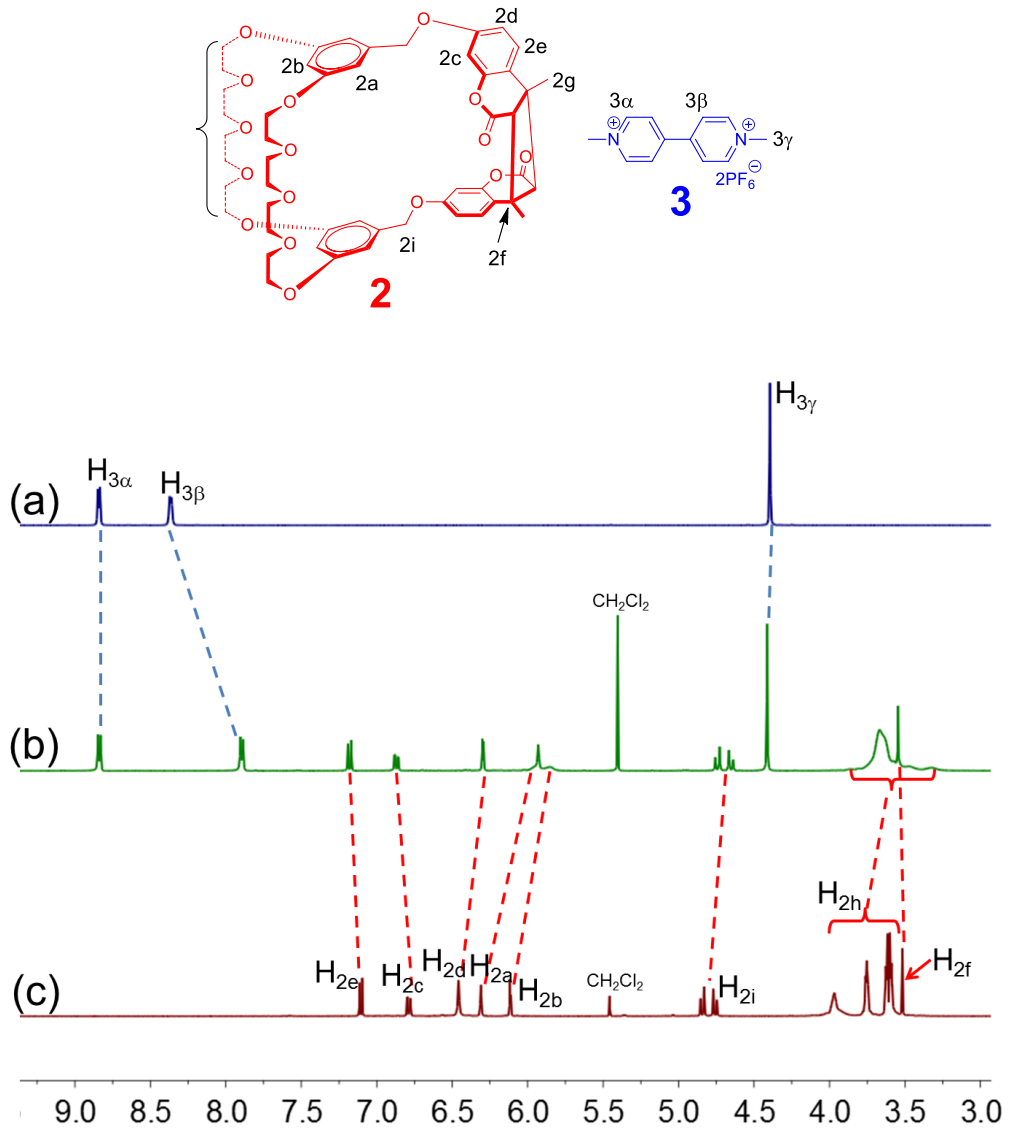

Fig. S27. Partial ^{1}H NMR spectra (500 MHz, $CDCl_3$, 293 K): (a) **3**; (b) **2**⊃**3**; (c) **2**. *c* = 5.00 mM.

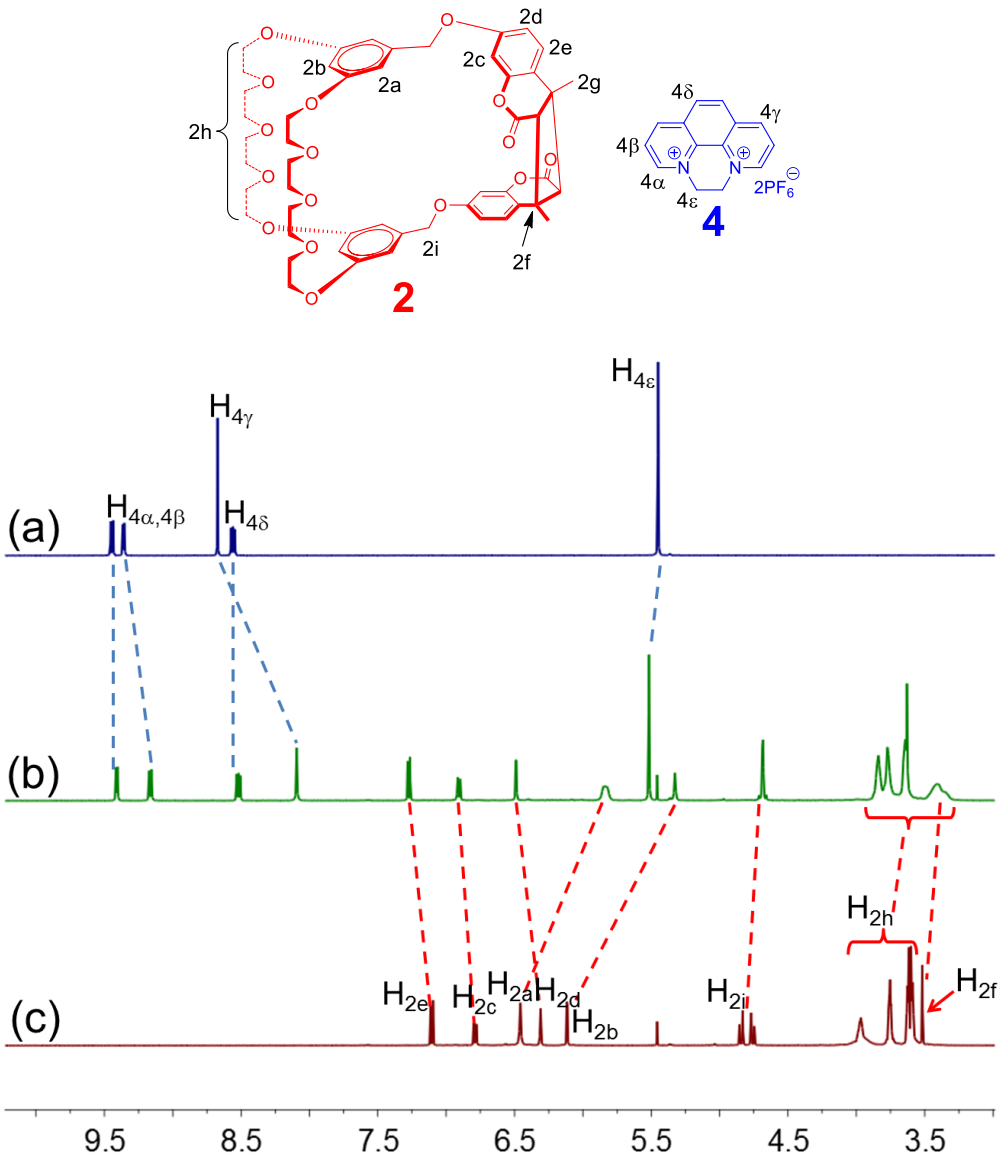

Fig. S28. Partial ^{1}H NMR spectra (500 MHz, $CDCl_3$, 293 K): (a) **4**; (b) **2**⊃**4**; (c) **2**. *c* = 10.0 mM.

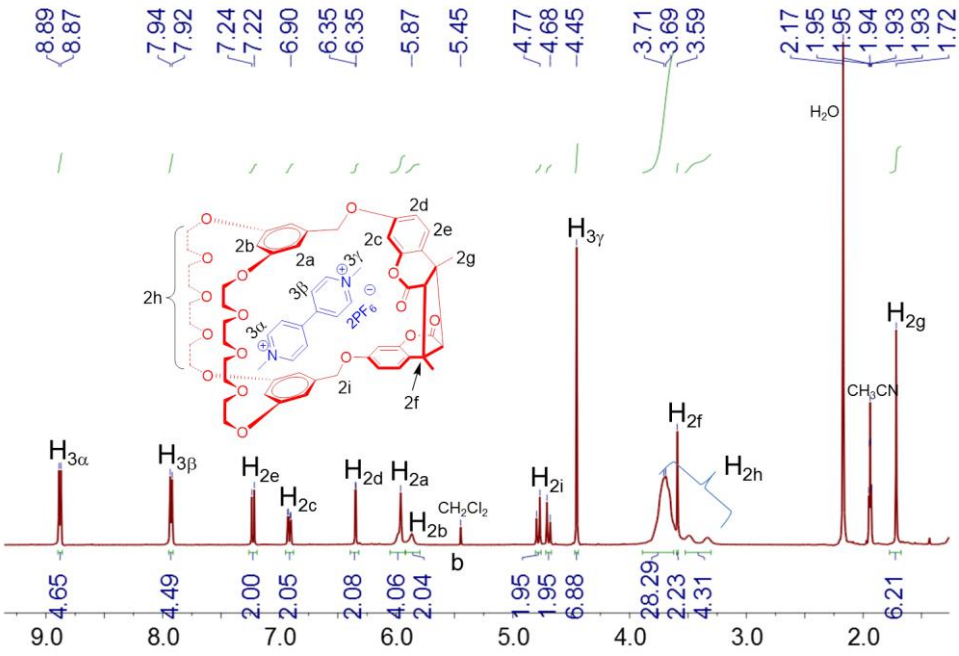

Fig. S29. Partial ^{1}H NMR spectrum (400 MHz, $CDCl_3$, 293 K) of **2⊃3**.

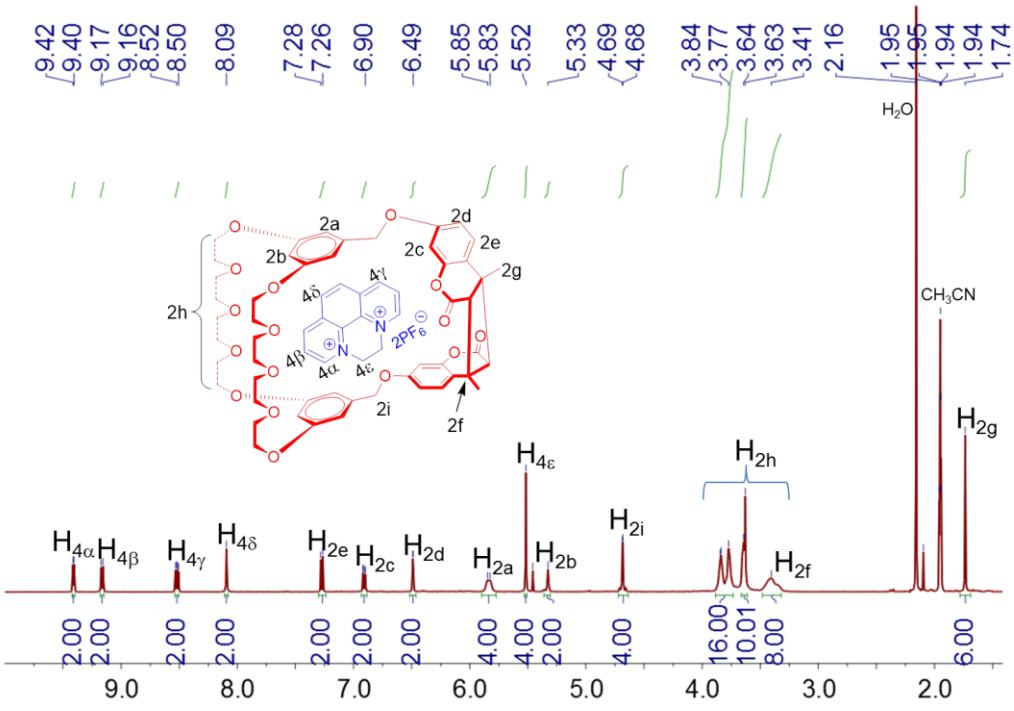

Fig. S30. Partial ^{1}H NMR spectrum (400 MHz, $CDCl_3$, 293 K) of **2⊃4**.

*5.3. Determination of association constants of complexes **2⊃3** and **2⊃4** in acetone*

The association constants (K_a) of complexes **2⊃3** and **2⊃4** were determined by probing the charge-transfer band of the complexes by UV-vis spectroscopy and employing a titration method. Progressive

addition of an acetone solution with high guest concentration and low host concentration to an acetone solution with the same host concentration resulted in an increase of the intensity of the charge-transfer band of the complex. Treatment of the collected absorbance data with a non-linear curve-fitting program afforded the corresponding association constants (K_a): (6.25 ± 0.36) × 10^3 M^{-1} for **2**⊃**3** and (1.11 ± 0.89) × 10^4 M^{-1} for **2**⊃**4**.

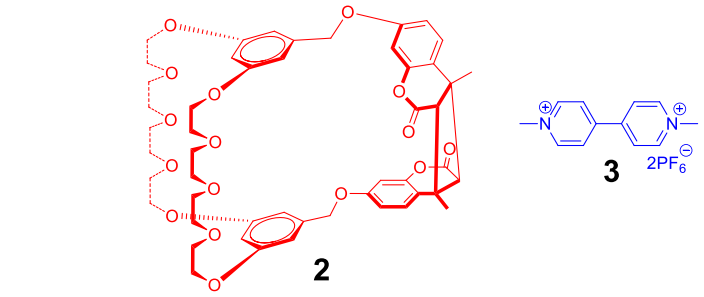

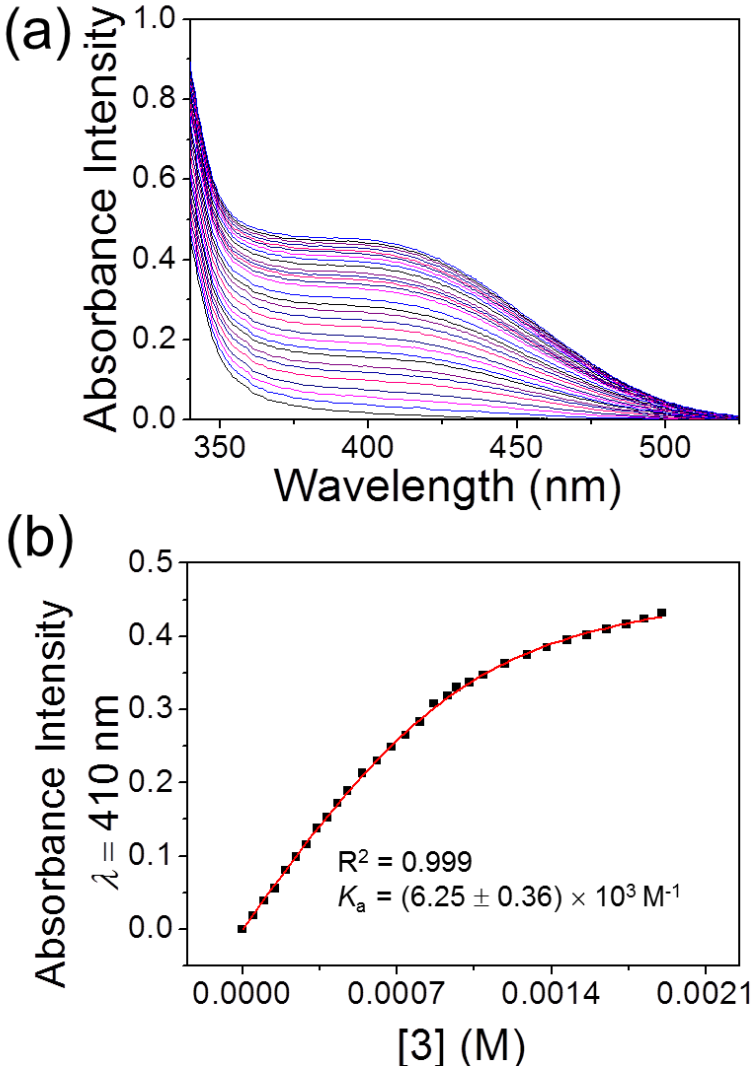

Fig. S31. (a) The absorption spectral changes of **2** (1.00 mM) upon addition of **3** and (b) the absorbance intensity changes at λ = 410 nm upon addition of **3** (from 0 to 1.90 mM). The red solid line was obtained from the non-linear curve-fitting using Eq. S1.

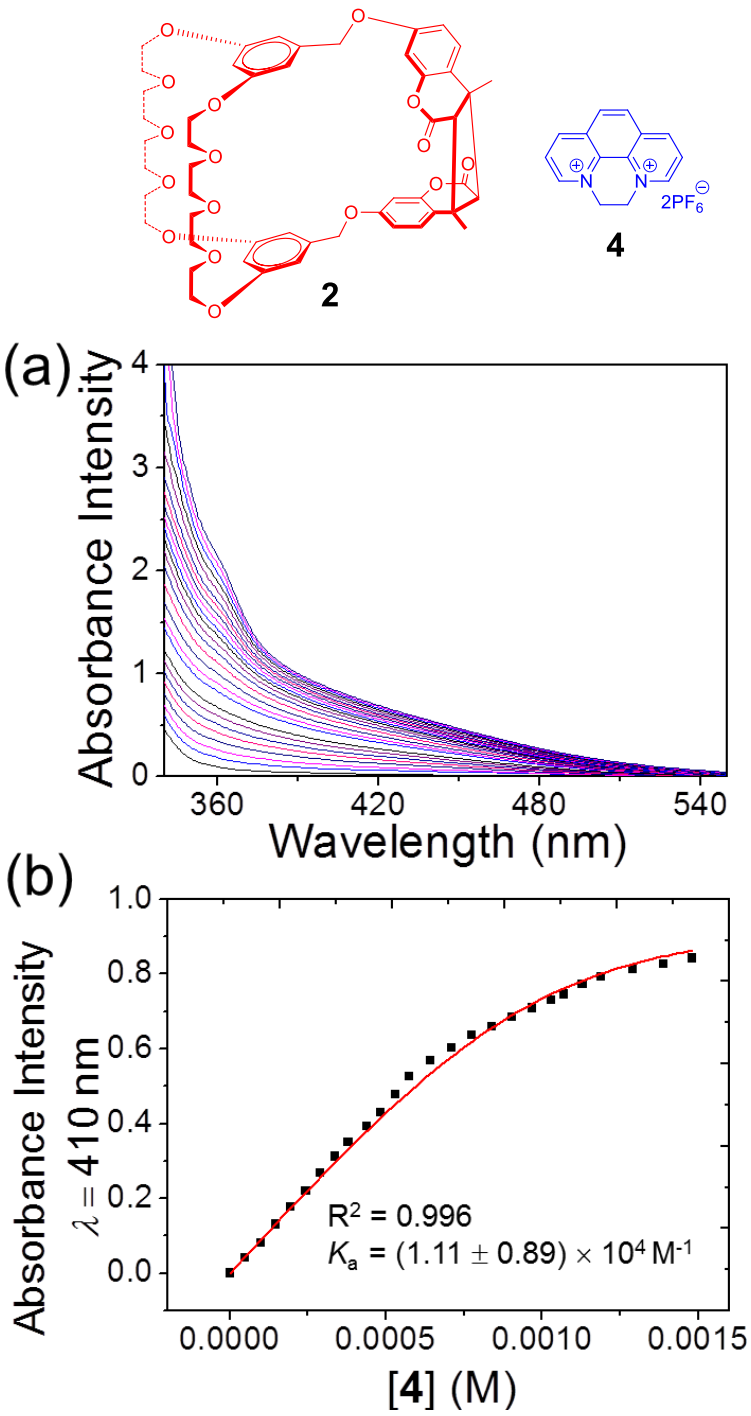

Fig. S32. (a) The absorption spectral changes of **2** (1.00 mM) upon addition of **4** and (b) the absorbance intensity changes at λ = 410 nm upon addition of **4** (from 0 to 1.50 mM). The red solid line was obtained from the non-linear curve-fitting using Eq. S1.

*6. X-ray analysis data for **1**⊃**4** and **2**⊃**3***

Crystallographic data for **1**⊃**4**: plate, yellow, 0.46 × 0.36 × 0.23 mm^3, $C_{148}H_{166}F_{24}N_{14}O_{33}P_4$, *FW* 3248.83, monoclinic, space group $P2_1/c$, a = 26.2806(15), b = 10.5229(5), c = 28.8376(16) Å, α = 90.00 °, β = 104.925(5) °, γ = 90.00 °, V = 7705.9(7) $Å^3$, Z = 2, D_c = 1.400g cm^{-3}, T = 170(2) K, μ = 0.156 mm^{-1}, 5744 measured reflections, 14066 independent reflections, 1019 parameters, 18 restraints, $F(000)$ = 3384, R_1 = 0.0799, wR_1 = 0.2039 (all data), R_2 = 0.1202, wR_2 = 0.2361 [$I > 2\sigma(I)$], max. residual density 0.755 e•$Å^{-3}$, and goodness-of-fit (F^2) = 1.033. CCDC 1506985.

Crystallographic data for **2**⊃**3**: plate, yellow, 0.49 × 0.40 × 0.26 mm^3, $C_{74}H_{87}F_{18}N_3O_{18}P_3$, *FW* 1741.38, triclinic, space group $P\bar{1}$, a = 12.9533(7), b = 13.4370(6), c = 26.4914(13) Å, α = 82.573(4) °, β = 79.383(5) °, γ = 65.221(5) °, V = 4107.7(4) $Å^3$, Z = 2, D_c = 1.408 g cm^{-3}, T = 170(2) K, μ = 0.180 mm^{-1}, 3771 measured reflections, 14962 independent reflections, 1054 parameters, 0 restraints, $F(000)$ = 1806, R_1 = 0.0994, wR_1 = 0.2748 (all data), R_2 = 0.2134, wR_2 = 0.3594 [$I > 2\sigma(I)$], max. residual density 1.482 e•$Å^{-3}$, and goodness-of-fit (F^2) = 1.025. CCDC 1506986.

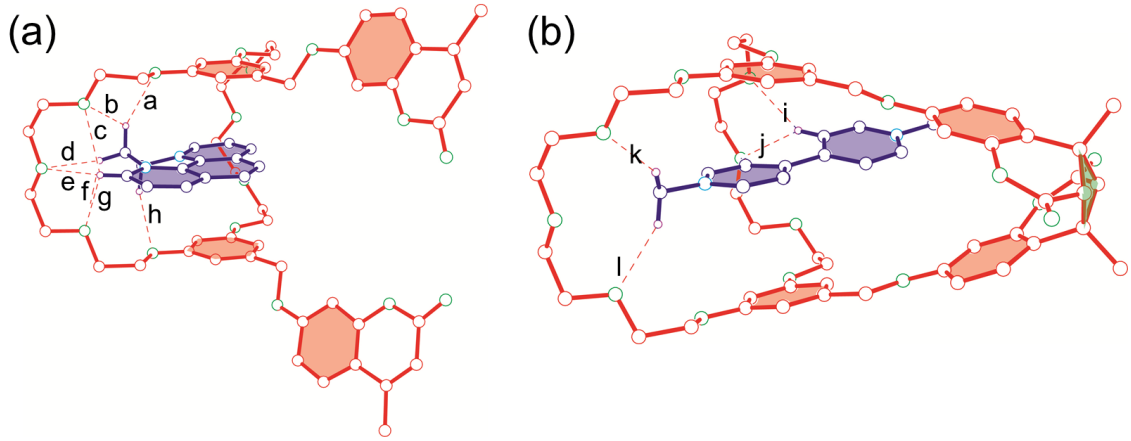

Fig. S33. Ball-stick views of the X-ray crystal structures of (a) **1**⊃**4** and (b) (**1**⊃**3**)@P = **2**⊃**3**. Hosts **1** and **2** are red, guests **3** and **4** are blue, hydrogens are purple, oxygens are green, and nitrogens are sky blue. PF_6^- counterions and hydrogens except the ones involved in hydrogen bonding were omitted for clarity. The green area in (b) denotes the cyclobutane ring produced from the cycloaddition reaction of two terminal coumarin moieties of **1**. Hydrogen bond parameters: C ··O distance (Å), H ··O distance (Å), C–H ··O angles (deg): **a**, 3.43, 2.65, 136; **b**, 3.07, 2.64, 106; **c**, 3.07, 2.92, 89.4; **d**, 3.39, 2.53, 145; **e**, 3.16, 2.26, 158; **f**, 3.31, 2.72, 118; **g**, 2.97, 2.63, 101; **h**, 3.45, 2.59, 146; **i**, 3.31, 2.47, 147; **j**, 3.51, 2.69, 146; **k**, 3.48, 2.58, 153; **l**, 3.43, 2.53, 153. Face-to-face π-stacking parameters between aromatic rings of **1** and **4**:

centroid-centroid distances (Å) 3.56, 3.60, 3.69, 3.82; ring plane/ring plane inclinations (deg): 1.68, 2.22, 5.19, 6.03. Face-to-face π-stacking parameters between aromatic rings of **2** and **3**: centroid-centroid distances (Å): 3.60, 3.88; ring plane/ring plane inclinations (deg): 7.91, 8.71.

References

S1. H. W. Gibson and D. S. Nagvekar, *Can. J. Chem.*, 1997, **75**, 1375–1384.

S2. Y. X. Shen, P. T. Engen, M. A. G. Berg, J. S. Merola and H. W. Gibson, *Macromolecules*, 1992, **25**, 2786–2788.

S3. X. Yan, X. Wu, P. Wei, M. Zhang and F. Huang, *Chem. Commun.*, 2012, **48**, 8201–8203.

S4. G. M. Sheldrick, *SHELXS-97, Program for solution of crystal structures*, University of Göttingen, Germany, 1990.

S5. G. M. Sheldrick, *SHELXS-97, Program for refinement of crystal structures*, University of Göttingen, Germany, 1997.